# Case study of a front refractivity signature with an operational radar and the Fabry algorithm modified for a magnetron transmitter

Besson Lucas[1], Frédéric Fabry[2], Jacques Parent du Châtelet[1]

[1]*Météo France, 11 bd d'Alembert, 78280 Guyancourt, France,*
*lucas.besson@latmos.ipsl.fr – jacques.parent-du-chatelet@latmos.ipsl.fr*

[2]*McGill University, 845 rue Sherbrooke O., Montreal, Canada, frederic.fabry@mcgill.ca*
(Dated: 30 May 2012)

**INSERT**

**PICTURE HERE**
Presenting author
Besson Lucas

## 1. Introduction

The ARAMIS operational radar network of Météo France deployed five S-band and 2 X-band over the Mediterranean Arc in the Southern region of France. This high coverage density is mainly due to the high occurrence of severe storms during the autumn season in this area. Moreover these severe storms are at the origin of the major part of the total annual rain in this region, leading to dramatic events such as fast floods, landslides … Observing, monitoring, and forecasting of these events are one of the principal task and objective of Météo France and of the RHYTMME[1] project.

The radar refractivity measurement, which is related to the fluctuation of water vapour, temperature and pressure at low level, is now implemented in this area on six radars (five S-band, and one 1 X-band). The purpose of the present case-study is to investigate the usefulness of the radar refractivity field for studying a moist air advection from the sea to the continent. The front observed the 16th October 2011 have been selected to be the case study. It has been observed by the radar of Nimes (S-band, Doppler, dual-polarisation).

In order to obtain refractivity field, the algorithm of Frédéric Fabry (University of McGill) has been used, after been adapted to take into account the constraint of the magnetron transmitter, whose frequency can drift with time. The refractivity fields during the event are confronted to the other measurement available (radar reflectivity, in situ measurements, analysis of the numerical weather prediction model AROME[2]). The primary results show that the refractivity fields are complementary to the others measurements, and seems provide further useful information for the localization and the propagation of the convective event.

## 2. Refractivity radar measurement

### 2.1. Basic equations for refractivity measurement with non-coherent transmitter

This section is detailed more precisely in Parent du Châtelet et al (submitted).

Following the formulation of Fabry (2004), the time delay $\tau_{travel}$ necessary for the electromagnetic wave to reach a target at distance r and come back to the radar is:

$$\tau_{\text{travel}}(r,t) = \frac{2}{c} \int_0^r n(x,t) \, dx = \frac{2r}{c} + \frac{2 \, 10^{-6}}{c} \int_0^r N(x,t) \, dx \qquad (1)$$

where $c$ is the speed of light in vacuum, $n(x,t)$ is the refractive index, and $N(x,t)$ is the refractivity at distance $x$ and at time $t$, defined by (Bean and Dutton, 1968):

$$N(x,t) = (n(x,t) - 1) \times 10^{-6} \qquad (2)$$

Variations of $\tau_{travel}$ due to refractivity changes can only be obtained through phase of the signal, and the purpose of this section is to establish the relationship between signal phase and refractivity changes for radar whose frequency can vary. The phase depends on the path travelled to the target, and also on transformations in the receiver.

The radar receiver has two identical channels for the received signal $S_{RX}(\tau)$, and for the transmitted signal $S_{TX}(\tau)$. Both are mixed with the same sinusoidal stable oscillator (STALO) $f_{LO}(t)$ provide I and Q zero frequency base-band complex signals $\mathbf{R_{RX}}(\tau)$ for the receive branch and $\mathbf{R_{TX}}(\tau)$ for the transmit branch. A digital AFC unit gives the phase $\varphi_{oT}$ for each transmitted pulse, and also measures the transmitted frequency f(t). The local oscillator is adjusted to follow the transmitted frequency variations, but the frequency $[f(t) - f_{LO}(t)]$ of the base-band signal is not exactly zero so that the phase of a signal received from a static isolated target also depends on the sampling time $\tau_{sam}$.

To take account of these points, the following development gives the formulation of the phase $\phi(\tau_{sam},t)$ for a signal transmitted at a frequency $f(t)$, backscattered by a isolated remote target located at range $r$, mixed with a sinusoidal local oscillator of frequency $f_{LO}(t)$, and sampled at a delay $\tau_{sam}$ after transmission. At the receiver input, the transmitted pulse $S_{TX}(\tau)$, and the signal $S_{RX}(\tau)$ received from the target after a delay $\tau_{travel}$, are given by:

---

[1] Risques HYdrométéorologiques en Territoires de Montagnes et MEditerranéens
[2] Applications de la Recherche à l'Opérationnel à MésoÉchelle

$$S_{TX}(\tau) = \cos\left[2\pi f(t)\tau + \varphi_{0TX}\right] \quad for\ \tau \in \left[0, \tau_{pulse}\right]$$

$$S_{RX}(\tau) = AS_{TX}(\tau - \tau_{travel}) = A\cos\left[2\pi f(t)(\tau - \tau_{travel}) + \varphi_{0TX}\right] for\ \tau \in \left[\tau_{travel}, \tau_{travel} + \tau_{pulse}\right]$$

(3)

where $\tau_{pulse}$ is the pulse duration and $\varphi_{oTX}$ is the transmitted phase. The constant A is for the target amplitude return.

At the receiver output, after multiplication by the local oscillator $LO(\tau) = \cos[2\pi f_{LO}(t)\tau - \varphi_{0LO}]$ and low pass filtering, we have:

$$R_{TX}(\tau) = I_{TX} + jQ_{TX} = \exp J\left[2\pi(f(t) - f_{LO}(t))\tau + \varphi_{0T}\right] \quad for\ \tau \in \left[0, \tau_{pulse}\right]$$

$$R_{RX}(\tau) = I_{RX} + jQ_{RX} = A\exp j\left[2\pi(f(t)\tau - f_{LO}(t)\tau - f(t)\tau_{travel} + \varphi_{0T}\right] for\ \tau \in \left[\tau_{travel}, \tau_{travel} + \tau_{pulse}\right]$$

(4)

Where $\varphi_{0T} = \varphi_{0TX} - \varphi_{0LO}$ is the measured transmitted phase for $\tau=0$.

$R_{RX}(\tau)$ is a sinusoidal signal of frequency $[f(t) - f_{LO}(t)]$ and duration $\tau pulse$. The signal is sampled at time $\tau_{sam}$, which is close, but not exactly equal, to $\tau_{travel}$. The measured phase $\phi(\tau_{sam},t)$ is given by the argument of $R_{RX}(\tau)$ for $\tau = \tau_{sam}$ and, after subtraction of $\varphi_{0T}$:

$$\varphi(\tau_{sam},t) = 2\pi\left(f(t)\tau_{sam} - f(t)\tau_{travel} - f_{LO}(t)\tau_{sam}\right) + \varphi_{t\,arg\,et}$$

(5)

Here $\phi, f, f_{LO}$ and $\tau_{travel}$ are all functions of the measurement time t.

To reveal the effects of refractivity variations, which are hidden in $\tau travel$, we define a "reference refractivity" $N_{ref}$ as the refractivity in reference conditions of temperature, pressure and humidity. Eq.(2) then becomes:

$$n(x,t) = 1 + 10^{-6}N(x,t) = 1 + 10^{-6}\left[N_{ref} + \delta N(x,t)\right]$$

(6)

Using Eq.(1), (5) and (6), we obtain:

$$\varphi(\tau_{sam},t) = 2\pi\left[-f_{LO}(t)\tau_{sam} + f(t)\Delta\tau - f(t)\Delta\tau_N(\tau_{sam},t)\right)\right]$$

$$with\ \Delta\tau = \tau_{sam} - \tau_{travel}(r, t_{ref}) = \tau_{sam} - \frac{2r}{c} - \frac{2r}{c}10^{-6}N_{ref}$$

(7)

$$and\ \Delta\tau_N(\tau_{sam},t) = \frac{2\times10^{-6}}{c}\int_0^r \delta N(x,t)dx$$

For each pixel, $\Delta\tau$ is a constant equal to the difference (mismatch) between the sampling time and the travel time under reference conditions. $\Delta\tau_N(\tau_{sam},t)$ is the supplementary propagation delay due to the difference of refractivity $\delta N(x,t)$ from the reference conditions.

Starting from Eq.(7), it is straightforward to obtain the expression for the difference $\Delta\phi(\tau_{sam},t,t_{ref})$ between phases measured at time $t$ and at a reference time $t_{ref}$, for signals both sampled at the same sampling time $\tau_{sam}$:

$$\Delta\varphi(\tau_{sam},t,t_{ref}) = 2\pi\begin{bmatrix} -\left[f_{LO}(t) - f_{LO}(t_{ref})\right]\tau_{sam} \\ +\left[f(t) - f(t_{ref})\right]\Delta\tau \\ -f(t_{ref})\Delta\tau_N(\tau_{sam},t) \end{bmatrix}$$

(8)

In the computation of the third term, we have neglected the phase contribution of $2\pi[f(t_{ref})-f(t)]\Delta\tau(\tau_{sam},t)$, equal to 3.6° for largest values of $f(t_{ref})-f(t)=500kHz$ and $\Delta\tau_N(\tau_{sam},t)= 0.02\mu s$.

Therefore the contributions of the variables are now completely separated: $f_{LO}(t)$ alone in the first term, $f(t)$ alone in the second term, and N(r,t) alone in the third term. As in Eq.(5), the phase difference $\Delta\phi$ is the sum of three terms, each of which is the product of a frequency by a time-delay:

- the first "**local oscillator term**" is the product of $[f_{LO}(t) - f_{LO}(t_{ref})]$ by $\tau_{sam}$. A correction is easy to achieve as long as the oscillator frequency $f_{LO}(t)$ is precisely known. An accuracy of 1 (in N units) leads to a phase change of 13°/km at C band. Using Eq.(8), a simple computation shows that it corresponds to a relative accuracy of 5 $10^{-7}$ on $f_{LO}(t)$. This can be easily obtained with a synthesizer synchronized by a thermostated reference;

- the second "**mismatch term**" is the product of $[f(t)-f(t_{ref})]$ by the constant $\Delta\tau$.

- the third "**refractivity term**" is the product of the constant $f(t_{ref})$ by $\Delta\tau_N(\tau_{sam},t)$ which is the difference, between times $t$ and $t_{ref}$, in the delay produced by the refractivity change from the reference. It is the classical expression of phase versus refractivity change.

## 2.2. Fabry Algorithm

The Fabry algorithm (Fabry et al, 1997, Fabry, 2004) is used to estimate a local refractivity. The method has been developed for coherent radar. As the ARAMIS network is only composed by non-coherent radar, the algorithm was modified to take in account the frequency drift. The formulation adapted to the frequency drift, described in the previous section, has been implemented in the algorithm. This study has also the objective to validate the use of the new algorithm version on the Météo France radar.

The algorithm is composed in two steps, the first one to obtain target calibration information, and the second one to estimate the local refractivity around the radar. The calibration step is focused on the identification of "good ground targets" and on the estimation of a refractivity reference $N_{ref}$. Then, the algorithm can estimate, for every ground target, a refractivity change between two PPI; and with the $N_{ref}$ map, a refractivity map around the radar.

The algorithm leads to correct the refractivity in function of the distance between the radar and the target. The objective is to decrease the aliasing risk, and so the error of the refractivity estimation.

It was successfully used in the United States during the IHOP campaign (Fabry, 2006) and elsewhere.

## 3. Case study

The 16th October 2012 is selected for the present study. This is a typical case of a moist air advection from the Mediterranean Sea to the continent.

The time evolution of the meteorological situation can be separation in three different steps:

- From 1100 to 1300 UTC: the atmosphere is impacted by the diurnal cycle. From an atmosphere relatively warm (~20°C) and dry (~40% of humidity), the diurnal cycle leads to an increase of the temperature and a decrease of the humidity;
- From 1300 to ~1600 UTC: the diurnal cycle is at its maximum, but no temperature and humidity variations are observed.
- From ~1600 to 1800 UTC: moist air coming from the sea advect over the Nîmes region. The humidity increases to 70-80% in a few hours. Moreover, the diurnal cycle is adding to this phenomenon, and the temperature is decreasing.

This case study is well document by the surface station of the RADOME network. Six surface stations are located in the area. This network is complete by the AROME analysis available every 3 hours (1200, 1500 and 1800 UTC for this study), and also by the radar of Nîmes. This radar is an S-band, Doppler, dual-polarisation of the ARAMIS network.

## 4. Comparison

In this section, we compare the refractivity measured by the magnetron radar to the refractivity calculated from AWS surface station (section 4.1) and calculated form AROME analysis (section 4.2).

### 4.1. Radar versus surface stations

The comparison is done at the location of each AWS. The Fabry algorithm allows calculating a local refractivity between two ground targets, and we must have ground targets located in the real vicinity of the AWS to insure that the comparison is meaningful. Around the radar, 4 surface stations are located within ground targets regions (30034002, 30209002, 30189001, 30258001), and 2 others are located at the limit of ground targets regions (30334003, 30258003). The surface station refractivity is calculated every hour from the equation $N = 77.6 \dfrac{P}{T} + 373000 \dfrac{e}{T^2}$.

The radar refractivity measurement is done through the algorithm for the entire time period (8 hours), and the gate corresponding to the surface station position is extracted.
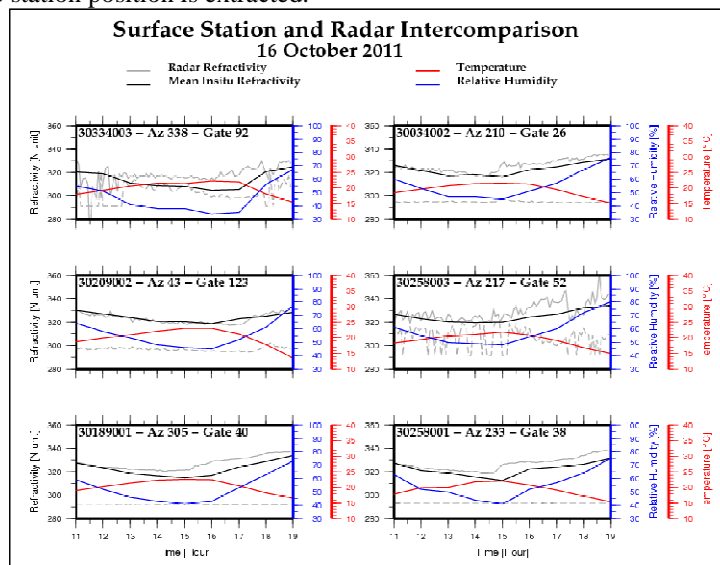


*Fig. 1 Comparison of refractivity time series for 6 AWS surface stations (in black) and the corresponding radar gate (in grey). The humidity and the temperature at the surface station are in blue and in red, respectively. The grey dash-line correspond to the error made on the radar measurement*

Figure 1 shows that the refractivity (radar and insitu) are in good agreement for stations situated within the ground echoes area (30034002, 30209002, 30189001 and 30258001). The radar is able to retrieve the time evolution of the refractivity, with an abrupt increase around the middle of the afternoon (from 1400UTC to 1700UTC – the time of this refractivity drift depends on the position of the AWS). This abrupt change is the consequence of the humidity increase in the low atmosphere (described in section 3).

However, we observed that the AWS time series are smoother than the radar ones. We also observe a more or less important time delay between radar and AWS time series particularly for stations 30189001, 30258001 and 30034002. This is due to the different sampling rate between radar (5 minutes) and AWS (1 hour measurements.

We observe a bias for some stations (30189001 and 30258001). It is probably due to our calibration method: we define the beginning of the analysed period (11h UTC) as the reference time, for which we suppose that the refractivity is homogeneous all over the area. This assumption is obviously not satisfied, regarding the scatter of AWS measurements at this time, larger than 10 (N unity).

Looking now to the measurements in the border areas of fixed echoes (Fig. 1, 30334003 and 30258003), we observe that radar and AWS measurements are not in agreement. The radar refractivity measurement can not be good, because, the target is not stable in time. Indeed, the error made on the radar measurement (gray dash line) is strong the major part of time.

Apart from this limitation, we can conclude that the radar refractivity, measured with the algorithm of Fabry, gives good results and allows identifying the advection of moist air on the continent.

### 4.2. Radar versus AROME analysis

As describe in section 3, AROME analysis are available at 1200, 1500 and 1800 UTC. Figure 2 illustrate the refractivity pattern from the radar (a, b and c respectively) and from the model (d, e and f respectively).
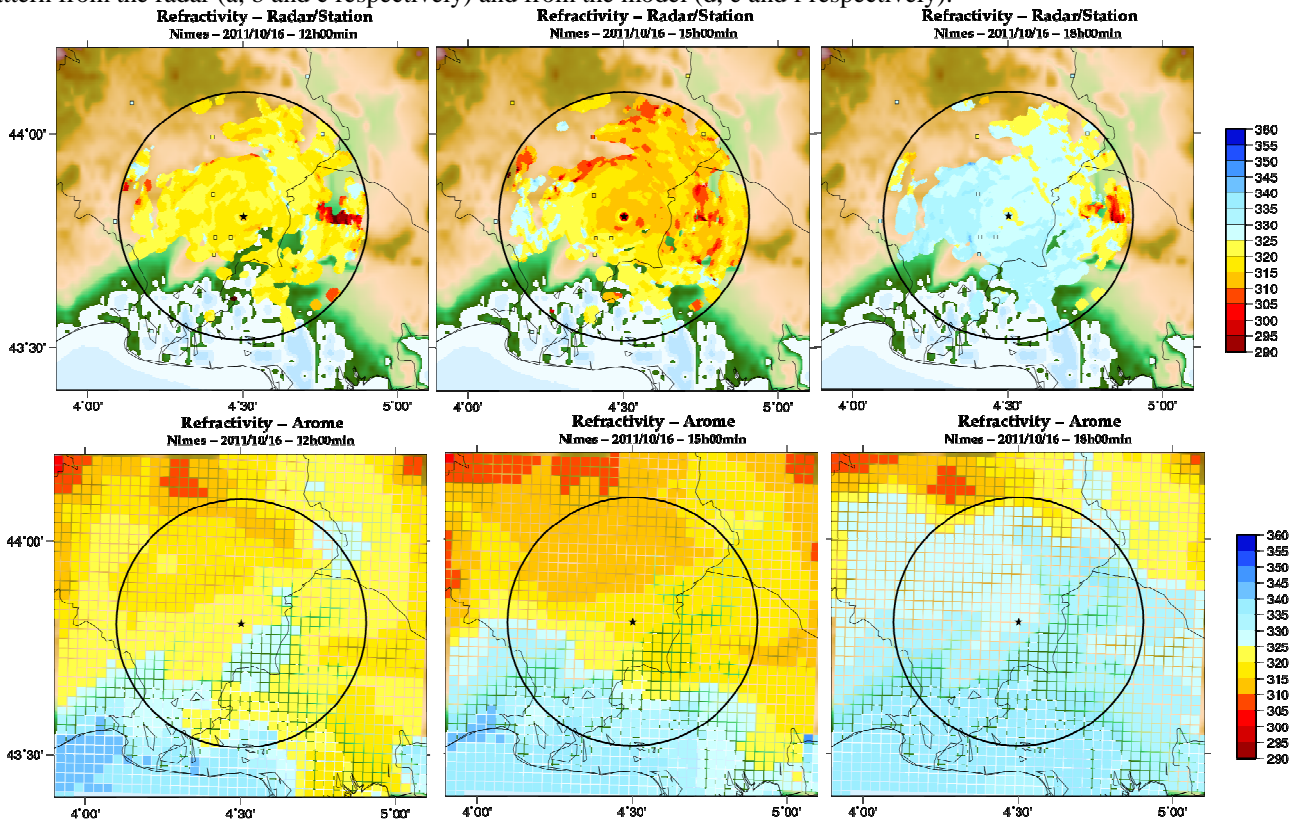


*Fig. 2 Refractivity map in the Nîmes region: from the radar (a) at 1200UTC, (b) 1500UTC and (c) 1800UTC, from AROME analysis (d) at 1200UTC, (e) at 1500UTC and (f) 1800UTC. The black circle correspond to the limit of the recording radar data (30 km from the radar), and the black star to the radar position*

At 1200 UTC (Fig. 2 a and d), refractivity fields are in accordance, comprised between 315 and 325 N units. Higher values of refractivity in the Camargue region in the AROME data (south of the domain) cannot be observed by the radar. Indeed, this region is a wetland, without useful ground targets by the algorithm. These high values of refractivity are generated by the advection of moist air from the sea.

In the Rhone valley (east of the radar), AROME analysis field also presents high refractivity values (~335 N units). This is not observed with the radar measurement, probably because AROME overestimates the surface fluxes, and of the evaporation generate by the Rhone River.

Eastward of the radar, low value of refractivity can be observed on the radar measurement. This artifact is probably due to a side lobe of the antenna. The algorithm of Fabry has a powerful processing to eliminate the side lobe effects, but it failed in

this case, due to the saturation of the ground echoes. The saturation leads to underestimate the ground target intensity, and so to underestimate the intensity of the side lobes.

At 1500 UTC (Fig. 2 b and e), the moist air advection can be both observed on the radar and AROME fields. Indeed, a high values area of refractivity is now present on the major part of the domain. The refractivity limit is less marked with the radar measurement. However, the increase of the refractivity, induced by the increase of the humidity, is visible.
The artifact is still present at the east side of the radar domain.

At 1800 UTC (Fig. 2 c and f), the two refractivity fields are identical. The advection of the moist air is now present over the whole domain. The higher refractivity values are present in the Rhone valley.
The artifact is still there!

The refractivity measurement from the radar is coherent with the refractivity analysis from AROME. Indeed, the global intensity of the refractivity, the time and the geographical evolutions are similar. Some differences can be noted, as side lobe elimination, are present.

## 5. Conclusions

Firstly, this case study is a supplementary validation of the new formulation of the refractivity equation to take into account the frequency drift of non-coherent radars. Indeed, the retrieved refractivities are in accordance with the refractivity measured by AWS. Moreover, the refractivity maps estimated with the radar are also in good accordance with the AROME analysis fields.
This study also highlights the possibility to use refractivity measurement to follow the transition between dry and moist air masses. Indeed, the refractivity increase induced by the increase of the humidity, well identified by AWS, is also observed with the radar. Thus the radar can map the refractivity at low level, and so give spatial information on the humidity field at low altitudes.
Future works will be based on the assimilation of the radar refractivity, particularly during the HyMeX campaign. Theses works are complete by in progress studies to improve the quality of the radar measurement by using the two available polarisation and by using other elevation angles in order to decrease the aliasing rate of the measurement.

## Acknowledgment

## References

Besson L, Boudjabi C, Caumont O, Parent du Châtelet J, 2012: Links between refractivity characteristics and weather phenomena measured by precipitation radar. *Bound-Lay Meteor*. **143**:77-95

Bringi V N and Chandrasekar V, 2001: Polarimetric Doppler Weather Radar. *Cambridge University Press: Cambridge.*

Fabry F, Frush C, Zawadzki I, Kilambi A, 1997: On the extraction of near-surface index of refraction using radar phase measurements from ground targets. *J Atmos Ocean Technol*. **14**:978-987

Fabry F, 2004: Meteorological Value of Ground Target Measurements by Radar. *J Atmos Ocean Technol*. **21**:560-573

Fabry F, 2006: The Spatial Variability of Moisture in the Boundary Layer and Its Effect on Convection Initiation: Project-Long Characterization. *J Atmos Ocean Technol*. **134**:79-91

Hubbert J-C, Dixon M, Ellis S M, G. Meymari, 2009a: Weather Radar Ground Clutter. Part I: Identification, Modeling, and Simulation. *J Atmos Ocean Technol*. **26**:1165-1180

Hubbert J-C, Dixon M, Ellis S M, 2009b: Weather Radar Ground Clutter. Part II: Real-Time Identification and Filtering. *J Atmos Ocean Technol*. **26**:1181-1197

Parent du Châtelet J., Boudjabi C, Besson L, Caumont O, submitted: Errors caused by long-term drifts of magnetron frequencies for refractivity measurement with a radar. Theoretical formulation and initial validation. *J Atmos Oceanic Technol.*

Parent du Châtelet J., Boudjabi C, 2008: A new formulation for a signal reflected from a target using a magnetron radar. Consequences for doppler and refractivity measurements. *5th European Conf Radar Meteorol Hydrol, Helsinky, Finland*, **ERAD**.

Smith E K Jr and Weintraub S, 1953: The constants in the equation for atmospheric refractive index at radio frequencies. *Proc. IRE*. **41**:1035-1037